



Combined DFT calculation, Hirshfeld surface analysis, and Energy framework study of non-covalent interactions in the crystal structure of (*Z*)-5-ethylidene-2-thiohydantoin determined by powder X-ray diffraction

Gerzon E. Delgado^{a,b,*}, Asiloé J. Mora^a, Luis E. Seijas^c, Luis Rincón^d, Gustavo Marroquin^e, Jonathan Cisterna^b, Alejandro Cárdenas^f, Iván Brito^b

^aLaboratorio de Cristalografía, Departamento de Química, Facultad de Ciencias, Universidad de Los Andes, Mérida 5101, Venezuela

^bDepartamento de Química, Facultad de Ciencias Básicas, Universidad de Antofagasta, Campus Coloso, Antofagasta 1240000, Chile

^cLaboratorio de Procesos Dinámicos en Química, Departamento de Química, Facultad de Ciencias, Universidad de Los Andes, Mérida 5101, Venezuela

^dGrupo de Química Computacional y Teórica and Instituto de Simulación Computacional, Universidad San Francisco de Quito, Quito 170901, Ecuador

^eEscuela Superior de Ingeniería Química e Industrias Extractivas, Instituto Politécnico Nacional, Zacatenco 07738, Ciudad de México, México

^fDepartamento de Física, Facultad de Ciencias Básicas, Universidad de Antofagasta, Campus Coloso, Antofagasta 1240000, Chile

ARTICLE INFO

Article history:

Received 17 January 2021

Revised 4 March 2021

Accepted 18 March 2021

Available online 26 March 2021

Keywords:

Powder X-ray diffraction

thiohydantoin

hydrogen bond patterns

NCI calculations

Hirshfeld surface analysis

Energy framework

ABSTRACT

The thiohydantoin core is used in the synthesis and development of new drugs. Furthermore, the study of these materials allows us to analyze the role that non-covalent interactions play in their supramolecular structure and how they can influence their pharmacological properties. Herein, a novel thiohydantoin compound, namely (*Z*)-5-ethylidene-2-thiohydantoin was synthesized and characterized by FT-IR, ¹H-NMR, and ¹³C-NMR spectroscopy. Its crystal structure was determined and refined by powder X-ray diffraction techniques. This material crystallizes in the monoclinic system with space group *P*2₁/*c*, *Z*=4. The crystal packing is controlled by N-H...O, N-H...S and C-H...O hydrogen bond interactions, forming infinite two-dimensional sheets with graph-set motifs R²₂(8), R¹₂(7), and R⁶₆(26). NCI calculations, Hirshfeld surface analysis, and the Energy framework study reproduce in good agreement the crystal packing exhibited by the X-ray diffraction study.

© 2021 Elsevier B.V. All rights reserved.

1. Introduction

Thiohydantoin and hydantoin are five-member heterocyclic compounds with a very reactive nucleus, which provides four possible points of diversity [1,2]. Due to the biological importance of this class of compounds, there has been interest in the development of new strategies for the synthesis of substituted hydantoins and thiohydantoins prepared more straightforwardly. Their molecular and crystalline structure has been studied, in solution and in the solid-state [3-5]. The biological activities of these materials have been known for a long time and are responsible for their wide range of therapeutic properties [6,7]. The best-known hydantoin, phenytoin, is the most widely used antiepileptic drug [8,9]. In particular, in the case of thiohydantoin (2-thioxo-imidazolidin-4-ones), the principal current interest comes from its recent application for the treatment of prostate cancers [10,11].

Both of these heterocycles, thiohydantoins and hydantoins, are commonly used as templates in combinatorial chemistry libraries [12], due to the possibility of forming simple building blocks to generate supramolecular architectures mainly based on the diverse and strong non-covalent interactions that can be formed. Precisely, in biological systems constituted by amino acids and their derivatives, the non-covalent interactions are key factors in their biological and chemical activity, particularly due to the formation of hydrogen bond interactions [13]. Thiohydantoins and hydantoins structural motifs, therefore, are suitable to form excellent supramolecular architectures through hydrogen bonds, which play a key role in molecular recognition and crystal engineering [14,15].

On the other hand, single-crystal X-ray diffraction is the most powerful technique for crystal structure determination of small molecules. However, when the intrinsic nature of the material is polycrystalline, or when a single crystal is not available, powder X-ray diffraction is the crystallographic tool to be used [16].

In this work, in continuation of our ongoing interest in the structural studies of thiohydantoin and hydantoin α -amino acid

* Corresponding author.

E-mail address: gerzon@ula.ve (G.E. Delgado).

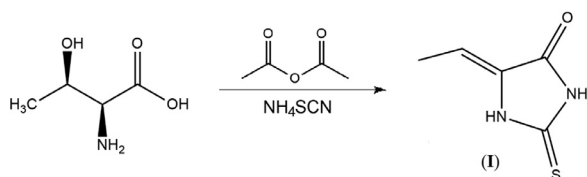


Fig. 1. Synthesis of (Z)-5-ethylidene-2-thiohydantoin (I).

derivatives [17–23], we analyze a new thiohydantoin crystal, obtained from a natural amino acid. We analyze the molecular and crystalline structure of the new compound (Z)-5-ethylidene-2-thiohydantoin, which was obtained from conventional X-ray powder diffraction data and refined by the Rietveld method. We consider this a good opportunity where non-covalent interactions, which exist within the crystal, can be discussed. The crystal three-dimensional hydrogen-bond network is examined here using powder X-ray diffraction. Furthermore, the nature of the non-covalent interactions existing in the crystal is analyzed through several theoretical methods and theories as DFT solid-structure optimization with NCI calculations, Hirshfeld surface and Energy framework analysis, and the main geometric characteristics rendered by this calculations were compared with those found from the crystallographic analysis.

2. Experimental Section

2.1. Synthesis

All the reagents used were purchased from commercial suppliers without further purification. Melting point determination was recorded using the Barnstead 9100 Electrothermal digital melting point apparatus. L-threonine (476.5 mg, 4.0 mmol) and NH₄SCN (304.5 mg, 4.0 mmol) were dissolved in a mixture of acetic anhydride (9 mL) and acetic acid (2 mL) (Fig. 1). This solution was warmed, with agitation, to 100°C over 1 hour, and then cooled to room temperature and stored in a freezer overnight. The resulting brown solid was collected by filtration and washed with cold water (m.p. 227–229°C).

2.2. Spectroscopic characterization (FTIR, ¹H-NMR, ¹³C-NMR)

The FT-IR absorption spectrum was obtained as KBr pellet using a Perkin-Elmer 1600 spectrometer. ¹H and ¹³C NMR spectra were determined on a Bruker Advance 400 model spectrometer, using DMSO-d₆ as solvent. FT-IR ν (cm⁻¹): 3233 and 3140 (N-H sp²), 2861 (C-H sp³), 1724 (C=O), 1673 (C=C), 1460 (C-N), 1186 (C=S). ¹H-NMR (400 MHz): δ 12.06 (s, 1H, N3-H3), 11.93 (s, 1H, N1-H1), 5.73 (c, 1H, C6-H6), 1.85 (d, 3H, C7-H7). ¹³C-NMR (100 MHz): δ 178.0 (C2, C=S), 164.1 (C4, C=O), 131.8 (C5, C-C), 111.6 (C6, C-H), 12.5 (C7-CH₃).

2.3. Powder X-ray diffraction

Powder X-ray diffraction experiments were performed at room temperature (295 K) using a Siemens D5005 diffractometer (40 kV, 30 mA) equipped with Ge<111> monochromated CuK α ₁ radiation ($\lambda = 1.54059$ Å). A small quantity of the sample was ground mechanically in an agate mortar and pestle. The resulting fine powder was mounted on a flat sample holder covered with a thin layer of petroleum jelly. The sample was spun about its normal at 15 r.p.m. and step scanned from 5° to 60° in 2θ , with a step size of 0.02° and counting time of 40 s. Quartz was used as an external standard.

The powder pattern revealed that the synthesized compound (I) was a single-phase and was indexed in a monoclinic cell with

$a = 4.0310(5)$ Å, $b = 16.087(3)$ Å, $c = 9.649(1)$ Å, $\beta = 95.00(1)^\circ$ using the program Dicolv04 [24], with figures of merit: $M_{20} = 76.9$ [25] and $F_{20} = 146.6(0.0038, 32)$ [26]. Evaluation of the systematic absences in the diffraction pattern indicated the space group $P2_1/c$ (No 14). The crystal structural solution was obtained by direct methods using the program EXPO [27]. All nine non-hydrogen atoms from the molecule were found in the E map of the best solution proposed by the EXPO program. The hydrogen atoms were placed in calculated positions. The model was refined by the Rietveld method [28] using the GSAS-II program [29]. Bragg reflections were modeled using a pseudo-Voigt peak shape function [30], and the background was fitted by the automatic interpolation of 10 points through the whole pattern. The powder pattern did not show preferred orientation, as can be seen in the well-modeled peaks in Fig. 2. Rotating the sample during data collection considerably reduces this problem. Therefore it was not necessary to apply this type of correction. Table 1 summarizes the crystal data, intensity data collection, and refinement details for the title compound (I). Experimental, calculated, and differences plot for the final Rietveld refinement cycle for compound (I) are shown in Fig. 2.

Crystallographic data for the structure reported here have been deposited with the Cambridge Crystallographic Data Centre (Deposition No. CCDC-1994886). These data can be obtained free of charge via www.ccdc.cam.ac.uk/data_request/cif. The Cambridge Structural Database (CSD, version 5.42, November 2020) was used for structure analysis [31].

2.4. NCI calculations

The Non-Covalent-Index (NCI) is based on the analysis of the electron density. This approach can highlight interactions on the low density, low gradient regime, and allowed us to identify different types of chemical interactions in terms of the electron density and its reduced gradient of density [32,33].

The molecular crystals have different types of non-covalent interactions that cannot be straightforwardly analyzed from direct inspection of the atom's position. The geometric characterization constitutes the first phase in the description of non-covalent interactions on the crystal structure, nevertheless, the relationship on the kind or strength of these interactions is not free of controversy [34]. So, the classification for the different types of non-covalent interactions based on pairwise distances and van der Waals radius could give systematic errors. Additionally, weak non-covalent interactions, such as dispersion interactions cannot be straightforwardly characterized by molecular orbital analysis. In such cases, a complementary topological analysis for the derived electron density is required. Many methods based on electron density have been proposed in recent years [35], as is the case of the Atoms in Molecules (AIM) theory [36,37]. In this theory, topological properties of electron density $\rho(\mathbf{r})$ can be employed for the quantitative assessment of weak interactions [38–41]. Laplacian of electron density can be written as the sum of contributions along the three principal axes of maximum variation, that is, $\nabla^2(\mathbf{r}) = \lambda_1 + \lambda_2 + \lambda_3$, where λ_i , are the eigenvalues of Hessian matrix. These eigenvalues allow the classification of critical points according to their rank, ω , number of non-zero curvatures at the critical point, and the sign of their algebraic sum of signs of the Hessian eigenvalues λ_i , σ : (ω, σ) . The bond critical point (3,-1) (BCP) is the most important type of critical point in the characterization of chemical interactions [34], there λ_3 varies along the inter-nuclear direction, whereas λ_1 and λ_2 vary in the plane perpendicular to λ_3 . Bonding interactions are associated with an electron density concentration in the inter-nuclear region. For covalent interactions negative contributions dominate and $\nabla^2(\mathbf{r}) < 0$, whereas for non-covalent interactions positive contributions dominate and $\nabla^2(\mathbf{r}) > 0$, with $\lambda_2 < 0$. In the particular case of hydrogen

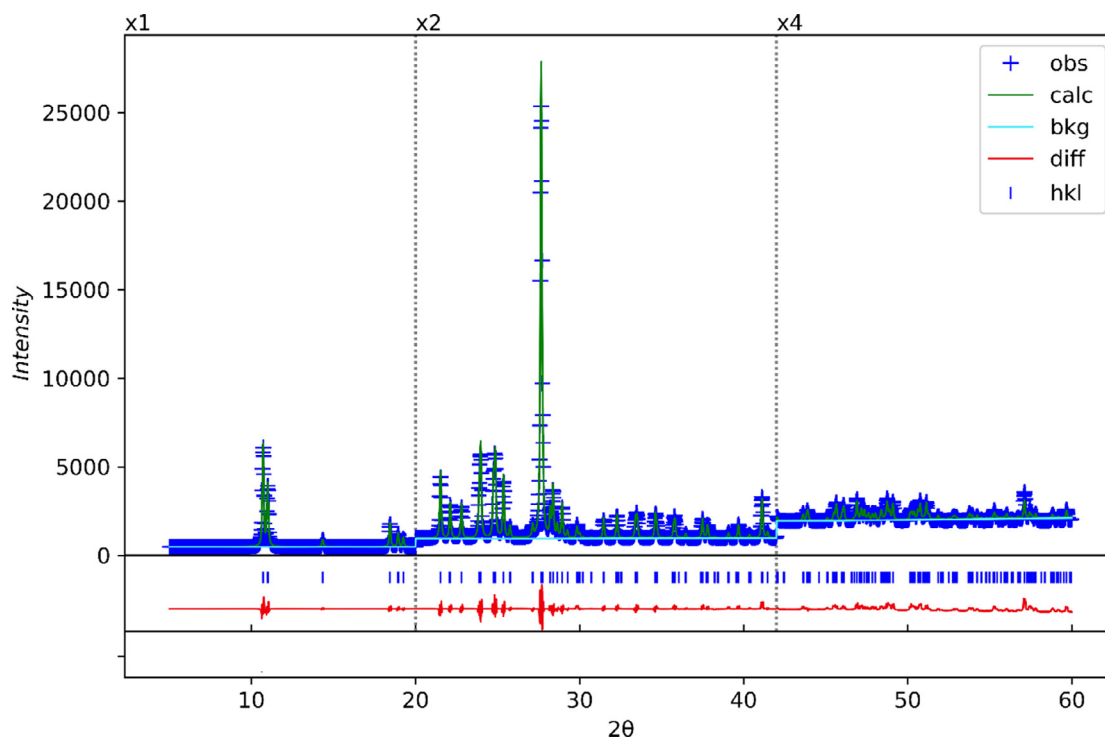


Fig. 2. Final Rietveld refinement plot for (I). The vertical scale of the 20° and 42° portions of the profiles has been multiplied by a factor of 2 and 4, respectively.

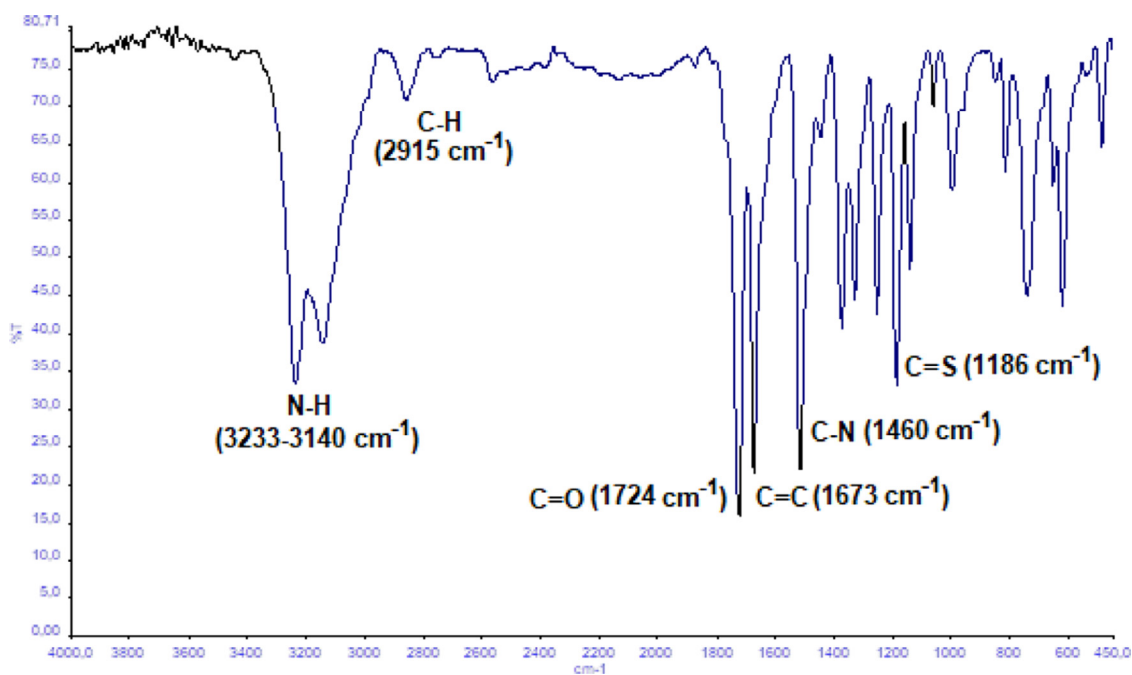


Fig. 3. FT-IR spectra of (I).

bonds, the electron density accumulation in the interatomic region, at BCP, is larger than the corresponding to van der Waals interactions.

Another classical alternative for non-covalent interaction characterization is the electron localization function (ELF) (eq 1), which depends on the difference between the total kinetic energy and the von Weizsäcker density functionals weighted by the Thomas-Fermi kinetic energy density functional through the localization index $\chi(\mathbf{r})$. This function yields the local excess of electron kinetic energy due to Pauli repulsion. In regions where electron pairs

are localized, Pauli repulsion has little significance. In consequence $\chi(\mathbf{r}) \rightarrow 0$ and $\eta(\mathbf{r}) \rightarrow 1$, allowing us to highlight the regions where electron localization occurs, which are associated with chemical interactions [41]. The ELF function represents a measure of the electron localization. Within the ELF representation, it is possible to find in a molecule two kinds of basins, core, and valence basins. The first ones are surrounding the nuclei. The other type of basins are characterized by the number of atomic valence shells in which they participate, in other words by the number of core basins with which they share a boundary, this is their synaptic order. In hy-

Table 1
Crystallographic data and experimental details for (**I**)

Chemical formula	C ₅ H ₆ N ₂ OS	CCDC	1994886
Formula weight	142.19	Diffractometer	Siemens D5005
Crystal system	monoclinic	Radiation [Å]	1.54059
Space group	P2 ₁ /c (N°14)	2θ range [°]	5–60
a [Å]	4.0307(3)	Step size (°)	0.02
b [Å]	16.0744(9)	Step time (s)	40
c [Å]	9.6457(8)	Structure determination	EXPO2014
β [°]	95.006(2)	Refinement method	Rietveld (GSAS-II)
V [Å ³]	622.6(1)	R _{exp}	0.040
Z	4	R _p	0.031
D _{cal} [g•cm ⁻³]	1.517	R _{wp}	0.049
Temperature [K]	295	χ ²	1.5

$$R_{\text{exp}} = 100 [(N-P+C) / \sum w(Y_{\text{obs}}^2)]^{1/2}$$

$$R_p = 100 \sum |Y_{\text{obs}} - Y_{\text{calc}}| / \sum |Y_{\text{obs}}|$$

$$R_{\text{wp}} = 100 [\sum w|Y_{\text{obs}} - Y_{\text{calc}}|^2 / \sum w|Y_{\text{obs}}|^2]^{1/2}$$

$$\chi^2 = [R_{\text{wp}} / R_{\text{exp}}]^2$$

drogen bonds two valence basins appear, one disynaptic basin associated with the bond electron pair in the donating group D-H and a monosynaptic basin associated with the acceptor lone pair. The ELF allows us to define localization domains, which contain all attractors bounded by an external isosurface with $\eta(\mathbf{r}) = f$. Successive reductions of localization domains, resulting from an increase in the f value, will split the parent domain into several domains, each one containing fewer attractors of the parent one. This split occurs at turning points located in the separatrix of two basins, originally involved in the parent domain. Ordering by increasing the value of f has been successfully employed to evaluate the HB strength [40,42].

$$\eta(\mathbf{r}) = (1 + \chi^2(\mathbf{r}))^{-1} \quad (1)$$

The recently non-covalent interaction (NCI) index developed by Jhanson *et al.*, use the reduced gradient (eq. 2) [32,33], in contrast to AIM which reveals covalent and non-covalent interactions, NCI identify the space regions where the non-covalent interactions take place, with the advantage of mapping the reduced gradient isosurfaces with a color scale based on electron density multiplied by the design of the second eigenvalue of the Hessian, allowing the identification of different interactions types, steric/repulsive ($\lambda_2 > 0$), Van-der-Waals like ($\lambda_2 \approx 0$), and attractive ($\lambda_2 < 0$).

$$s(\mathbf{r}) = \nabla \rho(\mathbf{r}) / 2(3\pi^2)^{1/3} \rho^{4/3}(\mathbf{r}) \quad (2)$$

To study the non-covalent interactions experimentally observed in the crystal structure, we used four structural models based on the crystal structure coordinates and without further geometry optimizations, to represent the most important non-covalent interactions in the crystal structure. The non-covalent interactions were assessed by the analysis of the DFT-CAM-B3LYP-D3BJ/6-311G++(d,p) [43,44] electron density $\rho(\mathbf{r})$ topology employing the Quantum Theory of Atoms in Molecule (QTAIM), the NCI-index (reduced gradient of $\rho(\mathbf{r})$) and the Electron Localization Function (ELF). For the QTAIM analysis, we use the AIMALL program [45], while the NCI-index calculations were carried out with NCIPLLOT program [41] and the ELF calculations were carried out with Multifn program [46]. All the isosurfaces were build up with VMD [47].

2.5. Hirshfeld surfaces

Hirshfeld surfaces of molecules in a crystal structure are constructed based on the electron distribution, which is calculated as the sum of spherical atom electron densities [48] and is unique

for each crystal [49]. The properties of the surface give information about the intermolecular interactions in the crystal. Each point on the Hirshfeld surface represents two distances: (1) the distance from this point to the nearest external nucleus (d_e) and (2) the distance to the nearest internal nucleus (d_i). Graphical plots of the molecular Hirshfeld surfaces are mapped with the normalized contact distance (d_{norm}), and these indicate regions of important intermolecular interactions [50]. The value of the d_{norm} is represented by red, white, or blue when the intermolecular contacts are shorter, equal, or longer to the van der Waals separation, respectively. The normalized contact distance d_{norm} , defined in terms of d_e , d_i and VdW radii of the atoms, was calculated using Eq. 1, where d_e and d_i are the distance from the Hirshfeld isosurface to the nearest external and internal nucleus, respectively, and VdW is the van der Waals radii of atoms taken from the literature [51].

$$d_{\text{norm}} = \frac{d_i - r_i^{\text{vdw}}}{r_i^{\text{vdw}}} + \frac{d_e - r_e^{\text{vdw}}}{r_e^{\text{vdw}}} \quad (3)$$

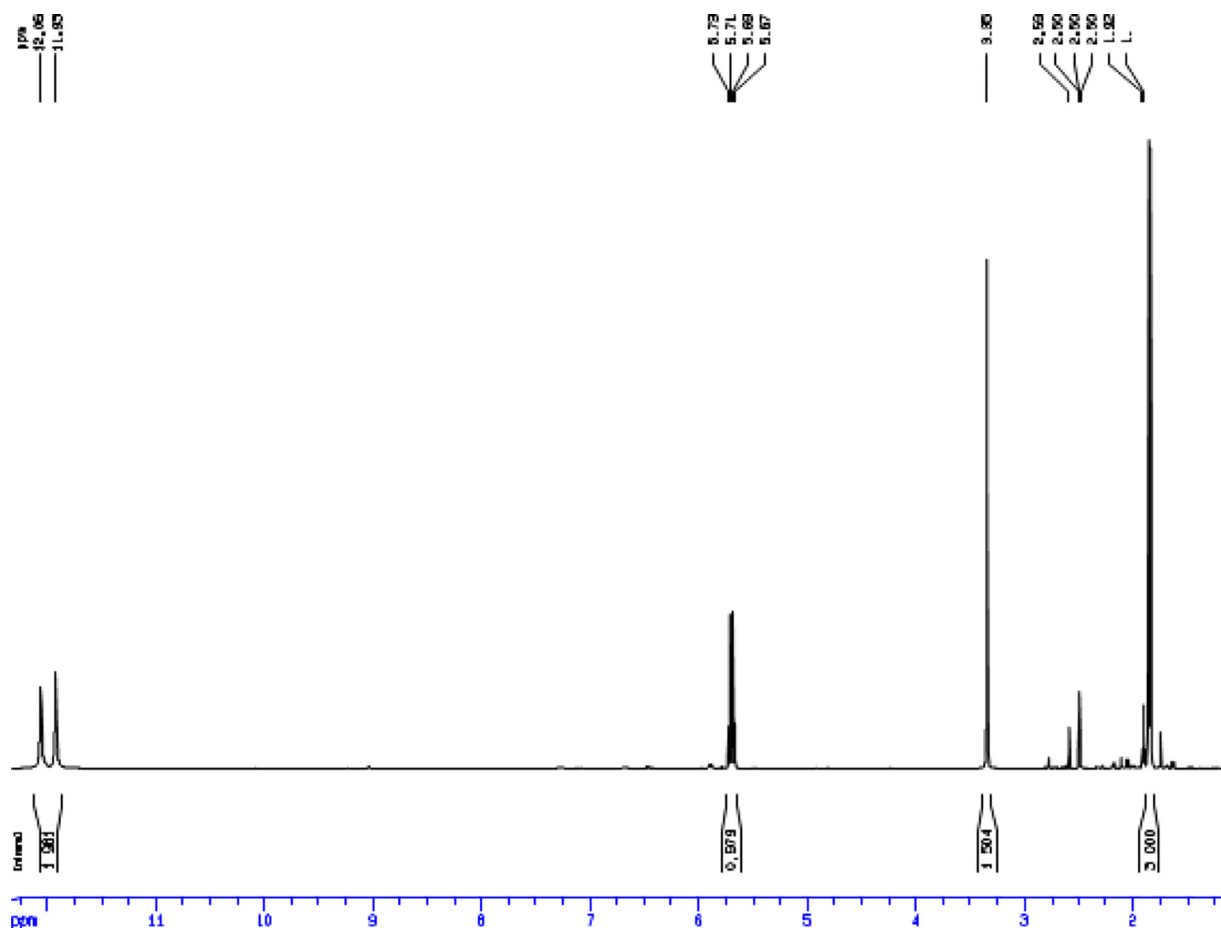
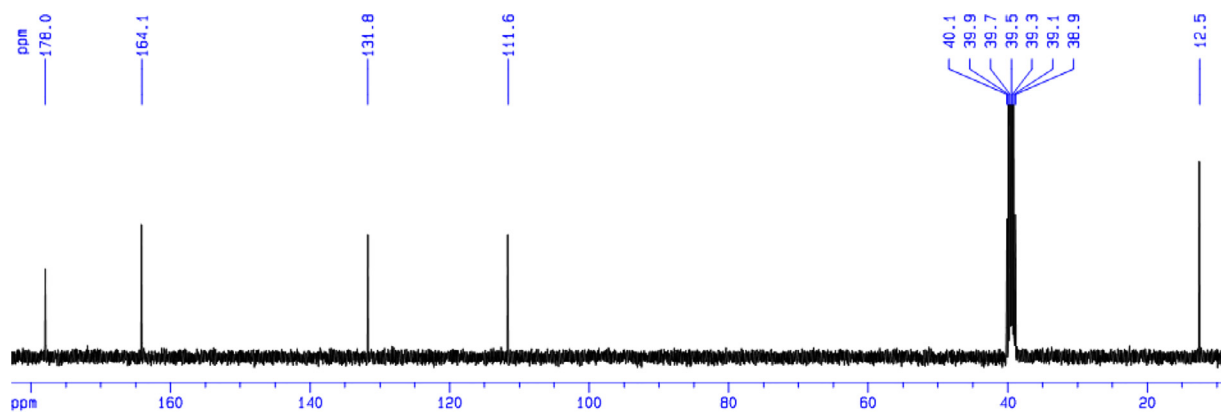
The combination of d_e and d_i in the form of a 2D fingerprint plot gives a summary of the intermolecular contacts in the crystal [52]. The fingerprint plots enable observation of contributions from different interaction types and it provides a valuable quantitative analysis of the intermolecular interactions occurring in the crystal structure. Moreover, quantification of energy framework energies is considered a powerful method for understanding the topology of the overall interactions of molecules in the crystal. This method allowed us to calculate and compare different energy components, i.e. repulsion (E_{rep}), electric (E_{ele}), dispersion (E_{dis}), polarization (E_{pol}), and total (E_{tot}) energy based on the anisotropy of the topology of pairwise intermolecular interaction energies.

For the title compound, an analysis of the Hirshfeld surfaces [48] was performed with the aid of CrystalExplorer17.5 software [53]. The two-dimensional fingerprint plots were calculated for the crystal, as were the electrostatic potentials [52]. The electrostatic potentials were mapped on the Hirshfeld surfaces using the 6-31G(d,p) basis set at B3LYP level of theory over a range of ± 0.002 au. The crystallographic information file (CIF) of (**I**) was used as input for the analysis. For the generation of fingerprint plots, the bond lengths of hydrogen atoms involved in interactions were normalized to standard neutron values (C-H = 1.083 Å, N-H = 1.009 Å, O-H = 0.983 Å).

3. Results and Discussion

3.1. FT-IR and NMR spectroscopic characterization

Spectroscopic studies confirm the molecular skeleton (see Fig. 1) of (Z)-5-ethylidene-2-thiohydantoin (**I**). Fig. 3 shows the FT-

Fig. 4. ^1H -NMR spectra of (I).Fig. 5. ^{13}C -NMR spectra of (I).

IR spectra where N-H, C-H, C=O, C=C, C-N, and C=S absorption bands in the regions of 3233 and 3140 cm^{-1} , 2915 cm^{-1} , 1724 cm^{-1} , 1673 cm^{-1} , 1460 cm^{-1} , and 1186 cm^{-1} , respectively were observed.

For (Z)-5-ethylidene-2-thiohydantoin (I) six signals are observed in the ^1H NMR spectra (Fig. 4) corresponding to N3-H3 in δ 12.64 (1H, s), C5-H5 in δ 4.57 (1H, d), C7-H methyl in δ 2.73 (3H, s), C8-H8 in δ 2.43 (1H, m), C9-H methyl in δ 1.09 (3H, d) and C10-H methyl in δ 0.77 (3H, d). The ^{13}C NMR spectrum (Fig. 5) of (I) displayed eight resonances including a thiocarbonyl C2 δ 183.0, two carbonyl group C4 δ 172.3 and C6 δ 169.7, C5 δ 66.7, C8 δ 29.0, C7 δ 27.3, C9 δ 17.4 and C10 δ 15.4. The COSY (Fig. 1S), HMBC (Fig.

Table 2
Hydrogen bonds geometry (\AA , $^\circ$) for (I).

D-H...A	D-H	H...A	D...A	D-H...A
N1-H1...O4 ⁽ⁱ⁾	0.860	2.000	2.854(5)	172
N3-H3...S2 ⁽ⁱⁱ⁾	0.860	2.550	3.399(4)	170
C7-H7A...O4 ⁽ⁱⁱⁱ⁾	0.960	2.400	3.352(5)	170

Symmetry codes: ⁽ⁱ⁾ $-1+x, \frac{1}{2}-y, -\frac{1}{2}+z$

⁽ⁱⁱ⁾ $1-x, -y, 1-z$

⁽ⁱⁱⁱ⁾ $-1+x, \frac{1}{2}-y, -\frac{1}{2}+z$

S2) and NOESY (Fig. S3) spectra confirm the Z configuration of the present thiohydantoin (I).

Table 3

Electron density topological properties in (3,-1) critical points found in structural models derived from the crystal structure of (Z)-5-ethylidene-2-thiohydantoin.

Interaction	CP	$\rho(\mathbf{r})$ (a.u.)	$\nabla^2(\mathbf{r})$ (a.u.)	λ_2 (a.u.)	H(r) (a.u.)	Ellipticity	ELF*
N1–H1...O4	(3,-1)	0.01892	0.09379	-0.02365	0.00437	0.013182	0.03932
N3–H3...S2	(3,-1)	0.01380	0.04152	-0.01283	0.00173	0.076212	0.06497
C7–H7A...O4	(3,-1)	0.01026	0.03492	-0.00961	0.00136	0.016159	0.03429
C6–H6...S2	(3,-1)	0.00407	0.01056	-0.00275	0.00520	0.05188	0.01918
S2...C7	(3,-1)	0.00344	0.01432	-0.00122	0.00091	0.434434	0.00699
H7B...H7C	(3,-1)	0.00307	0.01181	-0.00219	0.00074	3.812222	0.00688
N3...S2**	(3,-1)	0.00642	0.01765	-0.00250	0.00059	0.415658	0.02687
N1...C4**	(3,-1)	0.00529	0.01812	-0.00194	0.00065	0.267336	0.01469
O4...C5**	(3,-1)	0.00444	0.01530	-0.00119	0.00061	0.869834	0.01127
C6...H7A**	(3,-1)	0.00291	0.00947	-0.00126	0.00050	0.432932	0.00819

* ELF value evaluated at (3,-1) electron density CP;

** CP found in stack model.

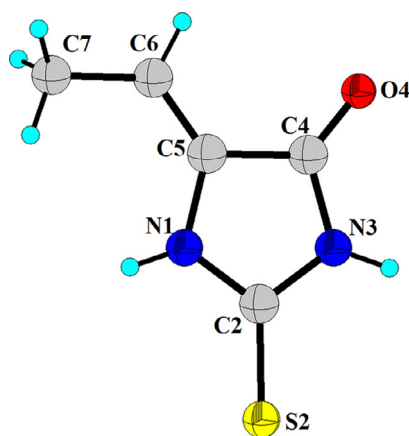


Fig. 6. The asymmetric unit of (I), showing the atomic numbering scheme; H atoms are shown as spheres of arbitrary radii).

3.2. Crystal and molecular structure

(Z)-5-ethylidene-thiohydantoin (I) crystallizes in a monoclinic cell with space group $P2_1/c$ with one molecule in the asymmetric unit. Fig. 6 shows the atom labeling and molecular conformation of the title compound. Supplementary material contains the fractional atomic coordinates and anisotropic temperature factors for non-hydrogen atoms, atomic positions and isotropic temperature factors for hydrogen atoms, and geometrical parameters as bond distances, bond, and torsion angles for (I).

All bond distances and angles are normal [54] and agree with the average values found in 33 entries with thiohydantoin ring fragments, found in the Cambridge Structural Database (CSD, version 5.42, November 2020) [31] with N1 and N3 unsubstituted. A search, including sp^2 hybridization at C5=C6 bond, showed 5 entries: AZADOV [55], CORZIT [56], MAKQEU [57], WOSLEV [58], and YINSUK [59]. The lengths of the C=S and C=O bonds are similar to those found in the two 2-thiohydantoin polymorphs [60,61] and all the entries with thiohydantoin found in CSD. The molecule is essentially planar, except for hydrogens H7B and H7C that are out of the plane, with a maximum deviation of -0.0059 Å in N3 and $+0.0058$ Å in C2.

In the crystal structure of (I) one intermolecular hydrogen bond interaction N1–H1...O4 ($-1+x, \frac{1}{2}-y, -\frac{1}{2}+z$) and two non-conventional N3–H3...S2 ($1-x, -y, 1-z$) and C7–H7A...O4 ($-1+x, \frac{1}{2}-y, -\frac{1}{2}+z$) interactions are observed (Table 2). The thioamide groups are linked into centrosymmetric dimers with graph-set motifs $R^2_2(8)$ [62] labeled A in Fig. 7. These hydrogen bonds form infinite sheets in the cb plane (Fig. 7), which are reinforced by the C–H...O interactions forming a new ring, with the O4 atom act as bifurcated accep-

tor, with graph-set $R^1_2(7)$ (labeled B in Fig. 7). Moreover, these hydrogen bonds form a macrocycle (hexamer) with graph-set $R^6_6(26)$ (labeled C in Fig. 7) with 6 molecules of (I) involved.

3.3. NCI calculations results

Trying to gain more insights into the characteristics of the non-covalent interactions in the crystal structure of (Z)-5-ethylidene-2-thiohydantoin (I), we performed an electron density topological analysis. In this analysis, we could identify 10 intermolecular interactions decreasing in strength from conventional and non-conventional hydrogen bonds to van der Waals interactions. Running along the $[2\ 0\ 1]$ and $[0\ -1\ 0]$ crystallographic directions we found a conventional N–H...O HB and N–H...S, C–H...O and C–H...S non-conventional HB interactions. Table 3 shows the principal electron density topological properties calculated for all the non-covalent (3,-1) bond critical point (BCP) found in the four structural models considered. In the first model, Fig. 8a, we could identify the three hydrogen N1–H1...O4, C6–H6...S2, C7–H7...O4. These HBs has a close shell bond nature, with $\nabla^2(\mathbf{r}) > 0$ and $H(\mathbf{r}) > 0$. Also from the same figure, we notice the acceptor bifurcated HBs with O4, with angles N,C–H...O4 of 172.2° and 170.1° for the N and C donors respectively. Fig. 8b, allows us to identify the N3–H3...S2 contact. This interaction has around the same electron density at BCP than the C–H...O HB and the triple of the C–H...S HB. A comparison between the topological parameters at BCP shows us that N–H...O has 27% more electron density at BCP than N–H...S. The ellipticity has been defined as $\varepsilon = |\lambda_1|/|\lambda_2| - 1$, where λ_1 and λ_2 are the negative eigenvalues of the electron density Hessian at the BCP. The ellipticity at the BCP can be interpreted as a measure in the anisotropy of the curvature in the normal directions to the bond path at the BCP. In the X–H...Y interactions we can observe an increase in the bond anisotropy following the order: N1–H1...O4 < C7–H7A...O4 < C6–H6...S2 < N3–H3...S2, the contacts X–H...S has the higher anisotropy, this is due to the high polarizability of the sulfur atom. Also, the title molecule (I) has two intramolecular weak contacts, H1...H7A and H6–O4, which are not associated with any BCP. This type of interaction is associated with an electron density distortion due to the presence of a second atom and corresponds to the steric clash entitled to the Z conformation in the molecule (I). The combination and periodical replication of the dimers showed in Fig. 8a and 8b, produce a supramolecular sheet showed in Fig. 9 in there we can observe two additional interactions associated with BCPs S2...C7 and H7B...H7C, these two interactions can be considered as attractive with $\lambda_2 < 0$ (see Table 3) and relative more ellipticity as X–H...Y interactions, this is due to the dispersion nature of this interactions. The stacking interactions are shown in Fig. 10. In there we can observe that these stacking interactions are largely delocalized between the molecules, also it is possible to observe the presence of intermolec-

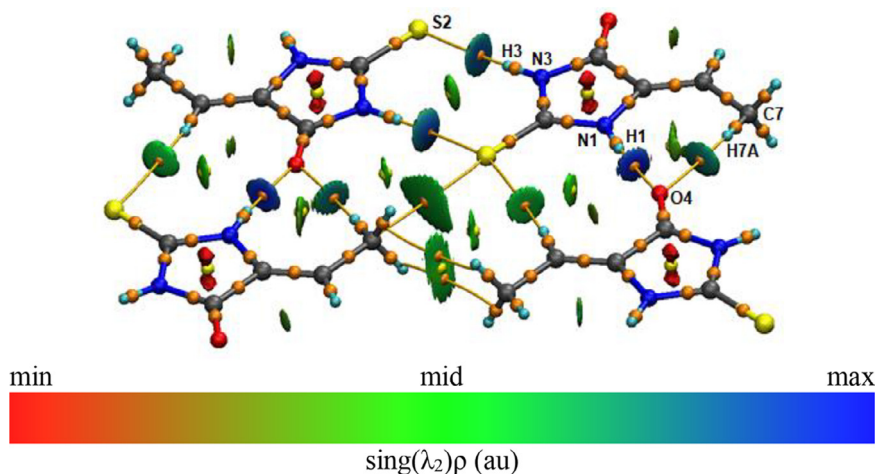


Fig. 9. Reduced gradient of density isosurface $s(\mathbf{r})=0.6399$, for the molecular sheet formed by the combination of dimer showed in [fig. 1](#). The isosurfaces were colored employing a color scheme for $\rho^* \text{sing}(\lambda_2)$ value been red for regions with $\lambda_2 < 0$ and blue $\lambda_2 > 0$ regions. The electron density critical points (3,-1) (orange) and (3,+1) (yellow) are shown.

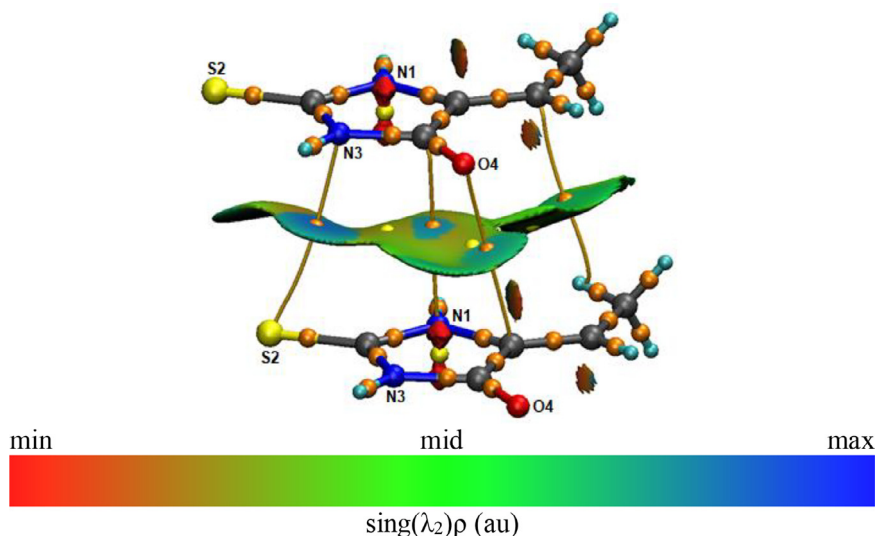


Fig. 10. Reduced gradient of density isosurface $s(\mathbf{r})=0.6299$, for the stacking interactions in (**I**). The isosurfaces were colored employing a color scheme for $\text{sing}(\lambda_2)\rho$ value been red for regions with $\lambda_2 < 0$ and blue $\lambda_2 > 0$ regions. The electron density critical points (3,-1) (orange) and (3,+1) (yellow) are shown.

ular BCPs. The delocalization of this interaction across the crystal structure is associated with cooperative effects, however, the quantification of these effects is still in intense debate [63].

3.4. Hirshfeld surfaces analysis

A Hirshfeld surface analysis was conducted to verify the contributions of the different intermolecular interactions. This analysis was used to investigate the presence of hydrogen bonds and other weak intermolecular interactions in the crystal structure. The plots of the Hirshfeld surface confirm the presence of the non-covalent interaction described below ([Fig. 11](#)), in very good agreement with the diffraction and NCI analyses.

To visualize and quantify the similarities and differences in intermolecular contacts across the crystal structure the Hirshfeld surface analysis was made with complementary analyses such as shape index and curvedness surface. For the title compound (**I**), the weak intermolecular interactions are mainly constituted by classical hydrogen bond interactions and some other weak interactions because of the centrosymmetric setting, the contributions are depicted in [Fig. 11a](#). The reciprocal contacts appear as an asymmetri-

cal broad wing for $\text{H}\cdots\text{C}$, with $d_e + d_i \simeq 3.3 \text{ \AA}$, for $\text{H}\cdots\text{N}$ as a broad spot with $d_e + d_i \simeq 3.5 \text{ \AA}$, the distance is greater than the van der Waals radii of N and H atoms ($d_e + d_i > 2.75 \text{ \AA}$) and, $\text{H}\cdots\text{O}$ as symmetrical sharp needles with $d_e + d_i \simeq 1.9 \text{ \AA}$. Another type of weak interaction is also observed in the Hirshfeld Surface analyses. For example, in this compound, the contribution of $\text{O}\cdots\text{C}$ and $\text{O}\cdots\text{N}$ with $d_e + d_i$ 2.4, 3.4 and, 3.4 \AA , respectively, could be owing to O (lone pair) $\cdots\pi$ (thiohydantoin) interaction as evidenced by the NCI plot in [Fig. 10](#). The oxygen interactions observed, corresponding to oxygen atoms of the title compound with an imidazoline ring. To the best of our knowledge, this is one of the first examples observed in the literature. The presence of this type of interaction is verified by a shape index plot in the molecule density ([Fig. 11b](#)).

On the other hand, the interatomic contacts of $\text{H}\cdots\text{H}$ interactions, show a broad triangular spot at diagonal axes $d_i + d_e \simeq 2.2 \text{ \AA}$ $\circ < 2.4 \text{ \AA}$, denoting $\text{H}\cdots\text{H}$ short contacts with another significant effect on the molecular packing.

The energy framework analysis helped us to a better understanding of the packing and topology of the crystal structure and the supramolecular rearrangement (see [Fig. 12](#)). According to the tube direction, it can conclude that the formation of the framework

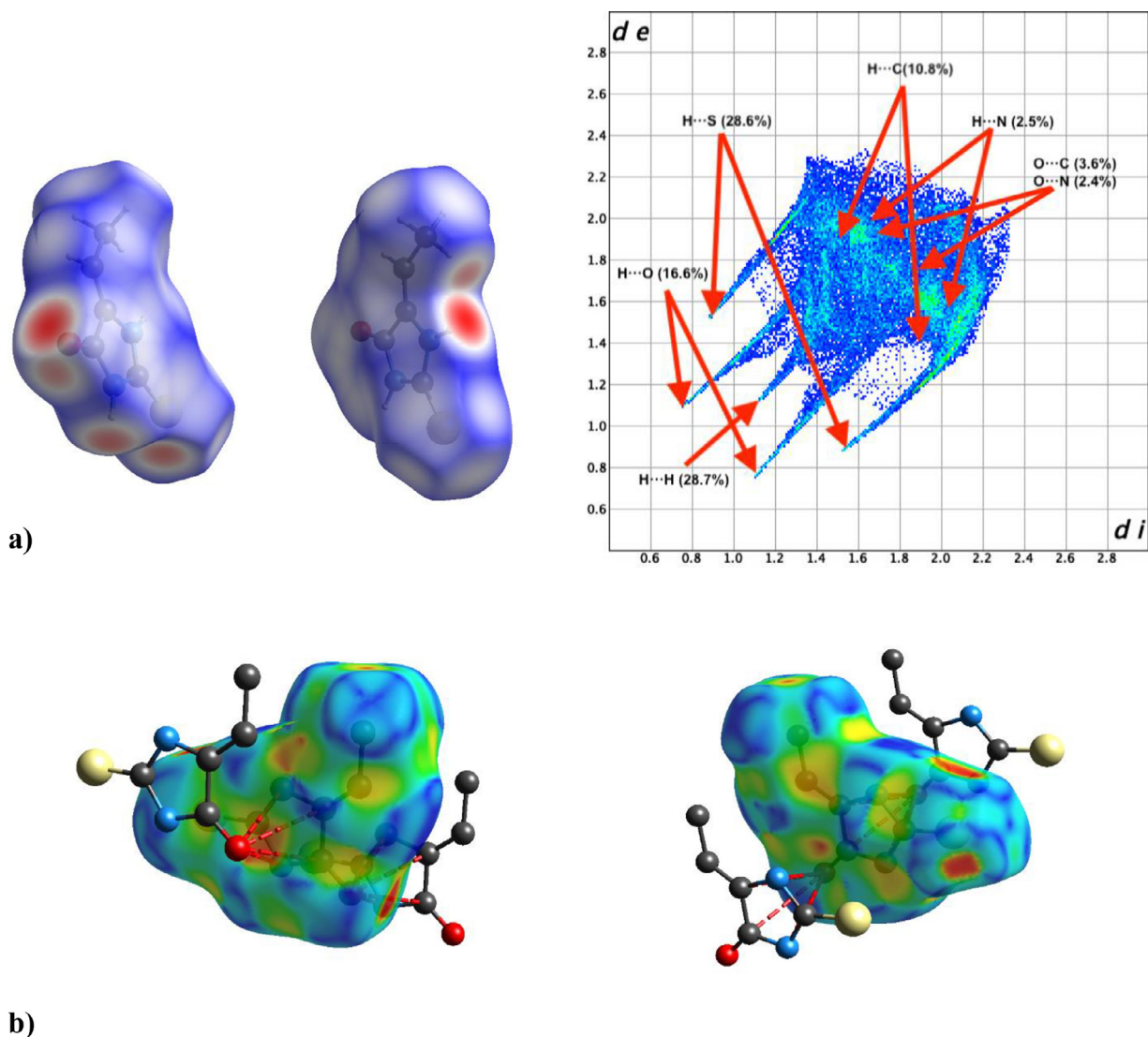


Fig. 11. Hirshfeld surface analysis and fingerprint plot (a) and, Shape index maps (b) of the title compound.

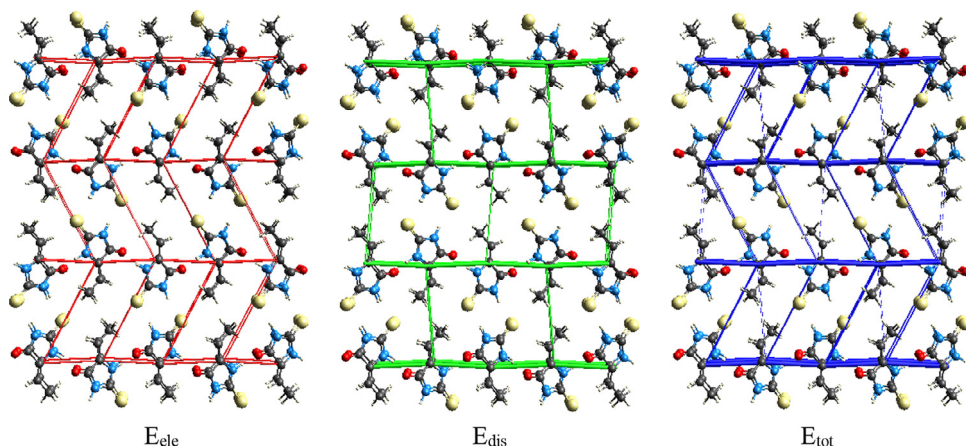


Fig. 12. Energy framework diagrams for E_{ele} , E_{dis} , and E_{tot} for title compound along the [100] direction.

is directed by the centrosymmetric setting for the title compound. This rearrangement allows the formation of other weak interactions to stabilize the crystal packing. The results of the calculations revealed that it exhibits dispersion interactions approximately parallel to the tube shape by the heterocycle in an antiparallel rearrangement through the b -axis with $-29.9 \text{ kJ}\cdot\text{mol}^{-1}$. The other en-

ergy components have values of $+18.7 \text{ kJ}\cdot\text{mol}^{-1}$, $-8.1 \text{ kJ}\cdot\text{mol}^{-1}$, and $-5.0 \text{ kJ}\cdot\text{mol}^{-1}$ for E_{rep} , E_{ele} , and E_{pol} , respectively. Energy framework diagrams show zig-zag ladder type and brick type topologies for electrostatic and dispersion energies, respectively (see Fig. 12). The small value of electrostatic energy versus dispersion energy in the title compound is attributed to the presence of weak classical hy-

drogen bond interactions. The total interaction energy that resulted from all four main components is $-24.3 \text{ kJ mol}^{-1}$.

4. Conclusions

With the need to explain in detail the wide-ranging nature of the many interactions that exist within a crystal, here we studied the non-covalent interactions in the new compound (Z)-5-ethylidene-2-thiohydantoin (**1**). Its crystal structure, determined by direct methods using conventional powder X-ray diffraction and refined by the Rietveld method, indicates that this material crystallizes in the monoclinic system, space group $P2_1/c$, with one independent molecule in the unit asymmetric. Hydrogen-bond analysis show that in the crystal structure, molecules are packed through intermolecular N-H...O, N-H...S, and C-H...O classical hydrogen bond interactions, which lead to the formation of infinite two-dimensional sheets in the *cb* plane with graph-set motifs $R^2_2(8)$, $R^1_2(7)$, and $R^6_6(26)$. The experimental structure was complemented with quantum chemical calculations as the NCI, Hirshfeld surfaces, and Energy framework study showing a good agreement with available experimental data. Hirshfeld surfaces and 2D fingerprint plots were used to clarify intermolecular interactions in the crystal lattice of the title molecule. The three-dimensional interaction energy analysis showed that the dispersion energy frameworks E_{dis} were slightly dominant over classical electrostatic terms E_{ele} .

Declaration of Competing Interest

The authors declare that they have no known competing financial interests or personal relationships that could have appeared to influence the work reported in this paper.

CRediT authorship contribution statement

Gerzon E. Delgado: Conceptualization, Supervision, Writing - original draft. **Asiloé J. Mora:** Conceptualization, Writing - review & editing. **Luis E. Seijas:** Software, Methodology. **Luis Rincón:** Software, Methodology. **Gustavo Marroquin:** Methodology. **Jonathan Cisterna:** Software, Supervision. **Alejandro Cárdenas:** Writing - review & editing. **Iván Brito:** Writing - review & editing.

Acknowledgements

This work was partially done into G.E. Delgado visit at the Universidad de Antofagasta, supported by MINEDUC-UA project, code ANT 1856. G.E. Delgado thank to FONACIT-Venezuela (grant LAB-97000821).

References

- C. Avendaño López, G. González Trigo, The chemistry of hydantoins, *Adv. Heter. Chem.* 38 (1) (1985) 177–228, doi:10.1016/S0065-2725(08)60920-4.
- M. Meusel, M. Gütschow, Recent developments in hydantoin chemistry. A review, *Org. Prep. Proced. Int.* 36 (5) (2004) 391–443, doi:10.1080/00304940409356627.
- G.G. Muccioli, J.H. Poupaerta, J. Wouters, B. Norberg, W. Poppitz, K.E. Gerhard, G.K. Scribad, D.M. Lamberta, A rapid and efficient microwave-assisted synthesis of hydantoins and thiohydantoins, *Tetrahedron* 59 (8) (2003) 1301–1307, doi:10.1016/S0040-4020(03)00033-4.
- Z.D. Wang, S.O. Sheikh, Y. Zhang, A simple synthesis of 2-thiohydantoins, *Molecules* 11 (10) (2006) 739–750, doi:10.3390/11100739.
- L. Konnert, E. Colacino, Recent advances in the synthesis of hydantoins: The state of the art of a valuable scaffold, *Chem. Rev.* 117 (23) (2017) 13757–13809, doi:10.1021/acs.chemrev.7b00067.
- S.H. Cho, S-H Kim, D. Shin, Recent applications of hydantoin and thiohydantoin in medicinal chemistry, *Eur. J. Med. Chem.* 164 (2) (2019) 517–545, doi:10.1016/j.ejmech.2018.12.066.
- L. Chen, Y. Hao, H. Song, Y. Liu, Y. Li, J. Zhang, Q. Wang, Design, synthesis, characterization, and biological activities of novel spirooxindole analogues containing hydantoin, thiohydantoin, urea, and thiourea moieties, *J. Agric. Food Chem.* 68 (39) (2020) 10618–10625, doi:10.1021/acs.jafc.0c04488.
- H.H. Merrit, T.J. Putnam, A new series of anticonvulsant drugs tested by experiments on animals, *Schweiz Arch. Neurol. Psychiatr.* 39 (5) (1938) 1003–1015, doi:10.1001/archneurpsyc.1938.02270050129007.
- J.M. Keppel Hesselink, D.J. Kopsky, Phenytoin: 80 years young, from epilepsy to breast cancer, a remarkable molecule with multiple modes of action, *J. Neurol.* 264 (8) (2017) 1617–1621, doi:10.1007/s00415-017-8391-5.
- M.E. Jung, S. Ouk, D. Yoo, C.L. Sawyers, C. Chen, C. Tran, J. Wongvipa, Structure-Activity relationship for thiohydantoin androgen receptor antagonists for castration-resistant prostate cancer (CRPC), *J. Med. Chem.* 53 (7) (2010) 2779–2796, doi:10.1021/jm901488g.
- J. Liu, B. Liu, Y. Jing, G. Zhao, Design, synthesis, and biological evaluation of thiohydantoin derivatives as novel anti-prostate cancer agents, *Anti-Cancer Agent* 16 (6) (2016) 740–746 <https://www.ingentaconnect.com/contentone/acamc/2016/00000016/00000006/art00009>.
- A.V. Bogolubsky, Y.S. Moroz, O. Savych, S. Pipko, A. Konovets, M.O. Platonov, O.V. Vasylychenko, V.V. Hurmach, O.O. Grygorenko, An old story in the parallel synthesis world: An approach to hydantoin libraries, *ACS Comb. Sci.* 20 (1) (2018) 35–43, doi:10.1021/acscombsci.7b00163.
- A.M. Maharromov, K.T. Mahmudov, M.N. Kopylovich, A.J.L. Pombeiro, *Non-covalent interactions in the synthesis and design of new compounds*, John Wiley & Sons, New Jersey, 2016.
- G.R. Desiraju, Hydrogen bridges in crystal engineering: Interactions without borders, *Acc. Chem. Res.* 35 (7) (2002) 565–573, doi:10.1021/ar010054t.
- G. Desiraju, *Crystal engineering: A brief overview*, *J. Chem. Sci.* 122 (5) (2010) 667–675 10.1007%2Fs12039-010-0055-2.
- W.I.F. David, K. Shankland, Structure determination from powder diffraction data, *Acta Cryst A* 64 (1) (2008) 52–64, doi:10.1107/S0108767307064252.
- L.E. Seijas, A.J. Mora, G.E. Delgado, M. Brunelli, A.N. Fitch, Study of the conversion of N-carbamoyl-L-proline to hydantoin-L-proline using powder synchrotron X-ray diffraction, *Powder Diffr* 25 (4) (2010) 342–348, doi:10.1154/1.3503660.
- G.E. Delgado, L.E. Seijas, A.J. Mora, Synthesis and crystal structure determination of hydantoin-L-proline, *J. Chem. Cryst.* 42 (9) (2012) 968–971, doi:10.1007/s10870-012-0344-3.
- L.E. Seijas, R. Almeida, A.J. Mora, G.E. Delgado, Cooperative effects on the formation of supramolecular synthons of thiohydantoin derivatives, *J. Comp. Meth. Sci. Eng.* 14 (1) (2014) 5–16, doi:10.3233/JCM-140480.
- G.E. Delgado, L.E. Seijas, A.J. Mora, R. Almeida, T. González, Crystal structure of 2-thiohydantoin-L-isoleucine synthesized under solvent-free conditions, *Mol. Cryst. Liq. Cryst.* 607 (1) (2015) 192–199, doi:10.1080/15421406.2014.928433.
- G.E. Delgado, J.A. Rodríguez, A.J. Mora, J. Bruno-Colmenárez, J. Uzcátegui, C. Chacón, Supramolecular structure of 5-methyl-5-phenyl hydantoin and hydrogen-bonding patterns in 5,5'-substituted hydantoins, *Mol. Cryst. Liq. Cryst.* 629 (1) (2016) 96–104, doi:10.1080/15421406.2015.1107745.
- L.E. Fernández, G.E. Delgado, L.V. Maturano, R.M. Tótaro, E.L. Varetta, Experimental and theoretical vibrational study of N-carbamoyl-L-proline, *J. Mol. Struct.* 1168 (1) (2018) 84–91, doi:10.1016/j.molstruc.2018.05.006.
- G.E. Delgado, A.J. Mora, L.E. Seijas, R. Almeida, C. Chacón, L. Azotla-Cruz, J. Cisterna, A. Cárdenas, I. Brito, N-acetyl-5-isopropyl-2-tioximidazolidin-4-one: Synthesis, spectroscopic characterization, crystal structure, DFT calculations, Hirshfeld surface analysis and energy framework study, *J. Mol. Struct.* 1219 (1) (2020) 128630 (12), doi:10.1016/j.molstruc.2020.128630.
- A. Boulif, D. Löuer, Powder pattern indexing with the dichotomy method, *J. App. Cryst.* 37 (5) (2004) 724–731, doi:10.1107/S0021889804014876.
- P.M. de Wolff, A simplified criterion for the reliability of a powder pattern indexing, *J. App. Cryst.* 1 (1) (1968) 108–113 <http://doi.org/10.1107/S002188986800508X>.
- G.S. Smith, R.L. Snyder, A criterion for rating powder diffraction patterns and evaluating the reliability of powder-pattern indexing, *J. App. Cryst.* 12 (1) (1979) 60–65 <http://doi.org/10.1107/S002188987901178X>.
- A. Altomare, F. Ciriaco, C. Cuocci, A. Falcicchio, F. Fanelli, Combined powder X-ray diffraction data and quantum-chemical calculations in EXPO2014, *Powder Diffr* 32 (S1) (2017) S123–S128, doi:10.1017/S088571561700015X.
- H.M. Rietveld, A profile refinement method for nuclear and magnetic structures, *J. Appl. Cryst.* 2 (2) (1969) 65–71, doi:10.1107/S0021889869006558.
- B.H. Toby, R.B. Von Dreele, GSAS-II: the genesis of a modern open-source all purpose crystallography software package, *J. Appl. Cryst.* 46 (2) (2013) 544–549, doi:10.1107/S0021889813003531.
- P. Thompson, D.E. Cox, J.B. Hastings, Rietveld refinement of Debye-Scherrer synchrotron X-ray data from Al_2O_3 , *J. Appl. Cryst.* 20 (2) (1987) 79–83 <http://doi.org/10.1107/S0021889887087090>.
- C.R. Groom, I.J. Bruno, M.P. Lightfoot, S.C. Ward, The Cambridge Structural Database, *Acta Cryst. B* 72 (2) (2016) 171–179, doi:10.1107/S2052520616003954.
- E.R. Jhonson, S. Keinan, P. Mori-Sánchez, J. Contreras-García, A. Cohen, W. Yang, Revealing non-covalent interactions, *J. Am. Chem. Soc.* 132 (18) (2010) 6498–6506, doi:10.1021/ja100936w.
- J. Contreras-García, E.R. Jhonson, S. Keinan, R. Chaudret, J.P. Piquemal, D.N. Beratan, W. Yang, NCIPLOT: a program for plotting noncovalent interaction regions, *J. Chem. Theory Comput.* 7 (3) (2011) 625–632, doi:10.1021/ct100641a.
- B. Lakshmi, A.G. Samuelson, K.V. Jovan Jose, S.R. Gadre, E. Arunan, Is there a hydrogen bond radius? Evidence from microwave spectroscopy, neutron scattering and X-ray diffraction results, *New. J. Chem.* 29 (2) (2005) 371–377, doi:10.1039/B411815D.
- G. Scoles (Ed.), *Atomic and molecular beam methods*, Oxford University Press, New York, 1992.

- [36] R.F.W. Bader, T.T. Nguyen-Dang, Quantum Theory of Atoms in Molecules–Dalton Revisited, *Adv. Quantum Chem.* 14 (1) (1981) 63–124, doi:[10.1016/S0065-3276\(08\)60326-3](https://doi.org/10.1016/S0065-3276(08)60326-3).
- [37] S.J. Grabowski, Relationships between QTAIM and the decomposition of the interaction energy–comparison of different kinds of hydrogen bond, in: C.F. Matta, R.J. Boyd (Eds.), *The quantum theory of atoms in molecules: from solid state to DNA and drug design*, Wiley, Darmstadt, 2017, doi:[10.1002/9783527610709.ch17](https://doi.org/10.1002/9783527610709.ch17).
- [38] L. Rincon, R. Almeida, D. García-Aldea, H. Diez y Riega, Hydrogen bond cooperativity and electron delocalization in hydrogen fluoride clusters, *J. Chem. Phys.* 114 (13) (2001) 5552–5562, doi:[10.1063/1.1351878](https://doi.org/10.1063/1.1351878).
- [39] J. Bruno-Colmenarez, R. Atencio, M. Quintero, L.E. Seijas, R. Almeida, L. Rincón, Crystal structure analysis and topological study of non-covalent interactions in 2,2-biimidazole: salicylic acid 2:1 co-crystal, *J. Chem. Cryst.* 47 (4) (2017) 47–58, doi:[10.1007/s10870-017-0679-x](https://doi.org/10.1007/s10870-017-0679-x).
- [40] A.J. Mora, L.M. Blandria, G.E. Delgado, L.E. Seijas, A. Lunar, R. Almeida, Non-covalent interactions in the multicomponent crystal of 1-aminocyclopentane carboxylic acid, oxalic acid and water: a crystallographic and a theoretical approach, *Acta Cryst. B* 73 (5) (2017) 968–980, doi:[10.1107/S2052520617011775](https://doi.org/10.1107/S2052520617011775).
- [41] M.E. Alikhani, F. Fuster, B. Silvi, What can tell the topological analysis of ELF on hydrogen bonding? *Struct. Chem.* 16 (6) (2005) 203–210, doi:[10.1007/s11224-005-4451-z](https://doi.org/10.1007/s11224-005-4451-z).
- [42] L.E. Seijas, L. Lunar, L. Rincón, R. Almeida, On the electron density localization in HF cyclic clusters, *J. Comput. Methods Sci. Eng.* 17 (1) (2017) 5–18, doi:[10.3233/JCM-160656](https://doi.org/10.3233/JCM-160656).
- [43] T. Yanai, D. Tew, N. Handy, A new hybrid exchange–correlation functional using the Coulomb-attenuating method (CAM-B3LYP), *Chem. Phys. Lett.* 393 (1–3) (2004) 51–57, doi:[10.1016/j.cplett.2004.06.011](https://doi.org/10.1016/j.cplett.2004.06.011).
- [44] S. Grimme, S. Ehrlich, L. Goerigk, Effect of the damping function in dispersion corrected density functional theory, *J. Comp. Chem.* 32 (7) (2011) 1456–1465, doi:[10.1002/jcc.21759](https://doi.org/10.1002/jcc.21759).
- [45] T.A. Keith, T.K. Gristmill, AIMAll version 19.10.12, Overland Park KS, USA, 2019. <http://aim.tkgristmill.com>.
- [46] L. Tian, C. Feiwu Chen, Multiwfn: A multifunctional wavefunction analyzer, *J. Comput. Chem.* 33 (5) (2012) 580–592, doi:[10.1002/jcc.22885](https://doi.org/10.1002/jcc.22885).
- [47] W. Humphrey, A. Dalke, K. Schulten, VMD - Visual Molecular Dynamics, *J. Molec. Graphics* 14 (1) (1996) 33–38, doi:[10.1016/0263-7855\(96\)00018-5](https://doi.org/10.1016/0263-7855(96)00018-5).
- [48] M.A. Spackman, P.G. Byrom, A novel definition of a molecule in a crystal, *Chem. Phys. Letters* 267 (3–4) (1997) 215–220, doi:[10.1016/S0009-2614\(97\)00100-0](https://doi.org/10.1016/S0009-2614(97)00100-0).
- [49] J.J. McKinnon, M.A. Spackman, A.S. Mitchell, Novel tools for visualizing and exploring intermolecular interactions in molecular crystals, *Acta Cryst B60* (12) (2004) 627–668, doi:[10.1107/S0108768104020300](https://doi.org/10.1107/S0108768104020300).
- [50] J.J. McKinnon, D. Jayatilaka, M.A. Spackman, Towards quantitative analysis of intermolecular interactions with Hirshfeld surfaces, *Chem. Comm.* 37 (1) (2007) 3814–3816, doi:[10.1039/B704980C](https://doi.org/10.1039/B704980C).
- [51] A. Bondi, van der Waals Volumes and Radii, *J. Phys. Chem.* 68 (3) (1964) 441–451, doi:[10.1021/j100785a001](https://doi.org/10.1021/j100785a001).
- [52] M.A. Spackman, J.J. McKinnon, Fingerprinting intermolecular interactions in molecular crystals, *CrystEngComm* 4 (66) (2002) 378–392, doi:[10.1039/b203191b](https://doi.org/10.1039/b203191b).
- [53] M.J. Turner, J.J. McKinnon, S.K. Wolff, D.J. Grimwood, P.R. Spackman, D. Jayatilaka, M.A. Spackman, *CrystalExplorer17*, University of Western Australia, 2017 <http://hirshfeldsurface.net>.
- [54] F.H. Allen, O. Kennard, D.G. Watson, L. Brammer, A.G. Orpen, R. Taylor, Tables of bond lengths determined by X-ray and neutron diffraction. Part 1. Bond lengths in organic compounds, *J. Chem. Soc., Perkin Trans. 2* (12) (1987) S1–S19, doi:[10.1039/P29870000051](https://doi.org/10.1039/P29870000051).
- [55] A.M. Asiri, H.M. Faidallah, A.O. Al-Youbi, T.R. Sobahi, S.W. Ng, Z)-2-Sulfanylidene-5-(thiophen-2-ylmethylidene) imidazolidin-4-one, *Acta Cryst E67* (9) (2011) o2429, doi:[10.1107/S1600536811033034](https://doi.org/10.1107/S1600536811033034).
- [56] W. Ksiazek, K. Kiec-Kononowicz, J. Karolak-Wojciechowska, Crystal and molecular structure of 5-benzylidene-2-thiohydantoin: The S...S intermolecular interactions between two C=S groups, *J. Mol. Struct.* 921 (1–3) (2009) 109–113, doi:[10.1016/j.molstruc.2008.12.060](https://doi.org/10.1016/j.molstruc.2008.12.060).
- [57] J.S. Casas, A. Castineiras, N. Playa, A. Sanchez, J. Sordo, J.M. Varela, E.M. Vazquez-Lopez, Methylmercury and dimethylthallium complexes of 5-(4'-dimethylaminobenzylidene)-2-thiohydantoin (HDABTd). The crystal and molecular structures of HDABTd and [TlMe₂(DABTd)(DMSO)], *Polyhedron* 18 (27) (1999) 3653–3659, doi:[10.1016/S0277-5387\(99\)00298-3](https://doi.org/10.1016/S0277-5387(99)00298-3).
- [58] M.M. Chowdhry, D.M.P. Mingos, A.J.P. White, D.J. Williams, Syntheses and characterization of 5-substituted hydantoins and thiazolines-implications for crystal engineering of hydrogen bonded assemblies, *J. Chem. Soc., Perkin Trans. 1* (20) (2000) 3495–3504, doi:[10.1039/B004312P](https://doi.org/10.1039/B004312P).
- [59] S.F. Brady, J.D. Bauer, M. Clarke-Pearson, R. Daniels, Natural products from isnA-containing biosynthetic gene clusters recovered from the genomes of cultured and uncultured bacteria, *J. Am. Chem. Soc.* 129 (40) (2007) 12102–12103, doi:[10.1021/ja075492v](https://doi.org/10.1021/ja075492v).
- [60] L.A. Walker, K. Foltz, L.L. Merritt, The crystal structure of 2-thiohydantoin, C₃H₄ON₂S, *Acta Cryst. B* 25 (1) (1969) 88–93, doi:[10.1107/S0567740869001804](https://doi.org/10.1107/S0567740869001804).
- [61] T. Ogawa, H. Okumura, M. Honda, M. Suda, S. Fujinami, A. Kuwae, K. Hanal, K.K. Kunitomo, A new polymorph of 2-thiohydantoin. 91–92. *X-ray Struct. Anal. Online* 25 (9) (2009) 91–92, doi:[10.2116/xraystruct.25.91](https://doi.org/10.2116/xraystruct.25.91).
- [62] M.C. Etter, J.C. MacDonald, J. Bernstein, Graph-set analysis of hydrogen-bond patterns in organic crystals, *Acta Crystallogr B46* (2) (1990) 256–262, doi:[10.1107/S0108768189012929](https://doi.org/10.1107/S0108768189012929).
- [63] M. Alonso, T. Woller, F.J. Martiñ-Martínez, J. Contreras-García, P. Geerlings, F. De Proft, Undertanding the fundamental role of p/p, s/s and s/p dispersion interactions in shaping carbon-based materials, *Chem. Eur. J.* 20 (17) (2014) 4931–4941, doi:[10.1002/chem.201400107](https://doi.org/10.1002/chem.201400107).